JCI The Journal of Clinical Investigation

Durable SARS-CoV-2 B cell immunity after mild or severe disease

Clinton O. Ogega, … , Andrea L. Cox, Justin R. Bailey

J Clin Invest. 2021. https://doi.org/10.1172/JCI145516.

Research In-Press Preview **Immunology** **Infectious disease**

Graphical abstract

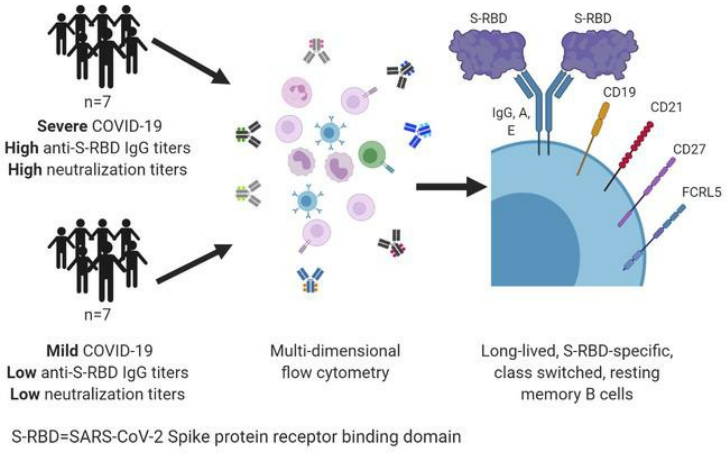

Durable SARS-CoV-2 B cell immunity after mild or severe disease

Clinton O. Ogega[1], Nicole E. Skinner[1], Paul W. Blair[1], Han-Sol Park[2], Kirsten Littlefield[2], Abhinaya Ganesan[2], Santosh Dhakal[2], Pranay Ladiwala[3], Annukka AR Antar[1], Stuart C. Ray[1], Michael J. Betenbaugh[3], Andrew Pekosz[2], Sabra L. Klein[2], Yukari C. Manabe[1], Andrea L. Cox[1,2], and Justin R. Bailey[1]*

Affiliations:

[1]Division of Infectious Diseases, Department of Medicine, Johns Hopkins University School of Medicine, Baltimore, Maryland, USA.

[2]W. Harry Feinstone Department of Molecular Microbiology and Immunology, The Johns Hopkins Bloomberg School of Public Health, Baltimore, Maryland, USA.

[3]Advanced Mammalian Biomanufacturing Innovation Center, Department of Chemical and Biomolecular Engineering, Johns Hopkins University, Baltimore, Maryland, USA.

Key words: SARS-CoV-2, COVID-19, neutralizing antibody, memory B cell

***Address correspondence to:**

Justin R. Bailey, MD, PhD
855 N. Wolfe Street
Rangos Building, Suite 520
Baltimore MD 21205, USA
Phone: 410-614-6087
Email: jbailey7@jhmi.edu

Conflict of interest statement. The authors declare that they have no conflicts of interest.

Abstract

Multiple studies have shown loss of SARS-CoV-2 specific antibodies over time after infection, raising concern that humoral immunity against the virus is not durable. If immunity wanes quickly, millions of people may be at risk for reinfection after recovery from COVID-19. However, memory B cells (MBC) could provide durable humoral immunity even if serum neutralizing antibody titers decline. We performed multi-dimensional flow cytometric analysis of S protein receptor binding domain (S-RBD)-specific MBC in cohorts of ambulatory COVID-19 patients with mild disease (n=7), and hospitalized patients with moderate to severe disease (n=7), at a median of 54 (39-104) days after symptom onset. We detected S-RBD-specific class-switched MBC in 13 of 14 participants, failing only in the individual with lowest plasma levels of anti-S-RBD IgG and neutralizing antibodies. Resting MBC (rMBC) made up the largest proportion of S-RBD-specific MBC in both cohorts. FCRL5, a marker of functional memory on rMBC, was more dramatically upregulated on S-RBD-specific rMBC after mild infection than after severe infection. These data indicate that most SARS-CoV-2-infected individuals develop S-RBD-specific, class-switched rMBC that resemble germinal center-derived B cells induced by effective vaccination against other pathogens, providing evidence for durable B cell-mediated immunity against SARS-CoV-2 after mild or severe disease.

Introduction

We are in the midst of an ongoing global pandemic caused by a novel coronavirus, SARS-CoV-2. COVID-19, the disease caused by SARS-CoV-2, can cause pulmonary inflammation, acute respiratory distress syndrome (ARDS), respiratory failure, and death. Despite the high morbidity and mortality caused by COVID-19, the majority of SARS-CoV-2-infected individuals recover and survive (1, 2). Following recovery, the durability of immunity against SARS-CoV-2 remains unclear. Durability of immunity is critical to mitigate the risk of reinfection for millions of people who have recovered or will recover from COVID-19.

After clearance of an infection or effective vaccination, phenotypically distinct B cell populations contribute to short- and long-term humoral immunity. Short-lived antibody-secreting cells (ASC) in blood and secondary lymphoid organs release antibodies into the circulation for weeks to months. Durable humoral immunity (lasting months to years) is mediated by bone marrow-resident, long-lived ASC and by memory B cells (MBC), which rapidly proliferate and differentiate into ASC in response to antigen re-challenge. Multiple studies have now demonstrated that serum antibody titers against SARS-CoV-2 wane and can even become undetectable after resolution of infection (3-6), likely reflecting a decline in short-lived ASC populations over time. Although other emerging reports have demonstrated more durable serum antibody responses (7-10), concerns remain that individuals who have recovered from COVID-19 may not maintain adequate immunity against reinfection. Individuals with mild COVID-19 disease generally mount lower titer antibody responses against the virus than those with severe disease (3, 10), raising particular concern that those who recover from mild infection are not protected against reinfection. If present and functional, MBC could provide durable humoral

immunity even after the loss of detectable serum antibody titers, as has been demonstrated after vaccination against viruses like hepatitis B virus (11, 12). However, Kaneko et al. showed a dramatic loss of germinal centers during acute COVID-19, raising concern that T cell dependent, durable, class-switched SARS-CoV-2-specific MBC responses may not reliably develop after SARS-CoV-2 infection (13).

Little is known about the frequency and phenotype of SARS-CoV-2-specific MBC that develop in response to either severe or mild infection. B cells specific for the SARS-CoV-2 Spike (S) protein have been isolated from individuals with very low antibody titers, but the relatively low frequency of these cells has thus far limited further characterization (14). We developed a highly sensitive and specific flow cytometry-based assay to quantitate circulating SARS-CoV-2 S protein receptor binding domain (S-RBD)-specific B cells, and a cell surface phenotyping panel to characterize these cells. We focused on S-RBD-specific B cells because most virus-neutralizing human monoclonal antibodies target this domain (14-18). Neutralizing activity has been associated with protection against reinfection by other coronaviruses (19-22), and protection against challenge in animal models of SARS-CoV-2 infection (23, 24). Therefore, S-RBD-specific B cells are likely to be the cells responsible for production of protective neutralizing antibodies upon re-exposure.

Classical markers applied to these S-RBD-specific B cells allowed us to identify B cell lineages including non-class-switched B cells, class-switched ASC, class-switched resting (classical) MBC (rMBC), activated MBC (actMBC), atypical MBC (atyMBC), and intermediate MBC (intMBC). Additional subpopulations were identified by staining for a chemokine receptor

(CXCR5), and potential inhibitory or activating receptors (FCRL5, CD22, and BTLA). Among the cell surface regulatory molecules, FCRL5 expression is of particular interest, since it is upregulated on long-lived antigen-specific rMBC that develop after effective vaccination against influenza and tetanus (25, 26). This FCRL5+ rMBC population prefentially expands and forms plasmablasts on antigen re-challenge, indicating that FCRL5 expression on antigen-specific rMBC is a marker of effective long-lived B cell-mediated immunity.

To investigate the potential for durable B cell immunity after SARS-CoV-2 infection, we analyzed S-RBD-specific B cells in ambulatory COVID-19 patients with mild disease and hospitalized patients with moderate to severe disease. We detected S-RBD-specific non-class-switched B cells, S-RBD-specific class-switched ASC, and/or S-RBD-specific class-switched MBC in all participants, regardless of their serum antibody titers or disease severity. We analyzed the frequencies of these S-RBD-specific B cell populations, and of S-RBD-specific MBC subsets, including rMBC, intMBC, actMBC, and atyMBC. By also quantifying cell surface molecules CD38, FCRL5, CD22, BTLA, and CXCR5 on these MBC populations and subsets, we identified a phenotypic profile of S-RBD-specific class switched MBC that was consistent with functional, durable B cell immunity.

Results

Selection of study participants.

B cells were obtained from participants with mild COVID-19 disease, moderate to severe disease, and from healthy COVID-19 negative controls (Table 1). Participants with mild COVID-19 disease who never required hospitalization or supplemental oxygen were identified in a previously described cohort of ambulatory patients (27). Symptoms in this cohort were tracked using a FLU-PRO score calculated from a participant survey, as previously described (27). To ensure that participants with mild disease were included in this study, a group of seven participants was selected with a median peak FLU-PRO score below the median peak score for the entire ambulatory cohort (FLU-PRO median (range)=0.09 (0.0-0.38) vs. 0.25 (0.0-1.63)). Seven additional participants with moderate to severe COVID-19 disease were selected from a second cohort of hospitalized patients (28), matched with the mild disease participants based on time since onset of symptoms at the time of blood sampling (median (range) time since symptom onset in days: ambulatory=61 (45-68); hospitalized=46 (39-104)). Peak supplemental oxygen support in hospitalized participants ranged from 2L via nasal cannula to mechanical ventilation. At the time of blood sampling for this study, five of the hospitalized participants had been discharged, and two remained hospitalized with critical illness. Hereafter, ambulatory, hospitalized, and healthy groups will be referred to as “mild”, “severe”, and “healthy”, respectively.

Quantitation of S-RBD-specific B cells.

A flow cytometry antibody panel was designed to identify non-class switched B cells (CD3-, CD19+, IgD/IgM+), class switched memory B cells (MBC) (CD3-, CD19+, IgM-, IgD-,

CD38+/- (excluding ++), CD138-) and class switched antibody secreting cells (ASC) (CD3-, CD27+, CD19+/-, IgM-, IgD-, CD38++) (Supplemental Figure 1). The frequency of all non-class switched B cells, class switched MBC, or class switched ASC among single viable lymphocytes was not significantly different between healthy, mild, and severe groups, but there was a trend toward greater frequency of class-switched ASC in the severe group compared to mild and healthy groups (Figure 1A).

As we defined these three B cell populations, we used a 6x-histidine (6xHis) tagged, soluble S-RBD protein followed by anti-His Alexa Fluor 647-conjugated antibody to stain cells expressing S-RBD-specific antibodies on their surface (Figure 1B and Supplemental Figure 1). To confirm that the 6xHis-S-RBD staining was specific, we compared frequency of S-RBD+ class-switched MBC measured using this protocol or by double staining with two different S-RBD proteins with two different tags (6xHis or mouse IgG1Fc) (Supplemental Figure 2). We detected binding of these two S-RBD proteins to B cells using anti-HIS-Alexa 647 and anti-mouse Fc-PE antibodies, respectively. We observed nearly identical nonspecific background S-RBD+ frequency from a healthy donor using our standard 6xHis antigen alone or double staining (0.012% positive by standard protocol and 0.012% positive by double staining protocol), and we also observed nearly identical S-RBD+ frequency from a COVID-19 patient using our standard 6xHis antigen alone or double staining (0.64% positive by standard protocol and 0.61% positive by double staining protocol) (Supplemental Figure 2). Therefore, we performed all subsequent staining with a single 6xHis-S-RBD antigen. We quantitated the frequency of S-RBD-specific cells among non-class switched B cells, class switched ASC, and class switched MBC (Figure 1C). Four of seven (57%) mild and seven of seven (100%) severe participants had a frequency of S-RBD-specific non-class switched B cells above the true positive threshold set using the healthy group. The

frequency of these cells did not differ significantly between the mild and severe groups. Since S-RBD specificity was detected by binding of S-RBD protein to cell surface immunoglobulin (Ig), detection of S-RBD-specific ASC was limited to the subset of immature ASC (plasmablasts) that had not yet downregulated surface Ig expression. Four of seven (57%) mild and four of seven (57%) severe participants had a frequency of S-RBD-specific class switched ASC above the true positive threshold. The frequency of these cells also did not differ significantly between the mild and severe groups. Six of seven (86%) mild and seven of seven (100%) severe participants had a frequency of S-RBD-specific class switched MBC above the true positive threshold. The single individual without detectable S-RBD-specific class switched MBC was asymptomatic throughout infection (peak FLU-PRO=0.0). Frequency of S-RBD-specific class switched MBC was significantly higher in severe participants than in mild participants (mean S-RBD+ frequency 0.85% vs. 0.20%, p=0.001). Taken together, these data demonstrate that S-RBD-specific cells could be detected among non-class switched B cells and class switched ASC in most SARS-CoV-2-infected participants, and S-RBD-specific class switched MBC could be detected in thirteen of fourteen participants. S-RBD-specific cells were significantly more frequent among class switched MBC from the severe group relative to the mild group.

Detectable S-RBD-specific MBC despite low levels of anti-S-RBD IgG and neutralizing antibodies in plasma.

Given concerns that low or waning plasma titers of neutralizing antibodies in some individuals indicate a lack of a durable humoral response, we were interested in evaluating whether COVID-19 participants with low levels of plasma anti-S-RBD IgG and low neutralizing antibody levels had detectable S-RBD-specific MBC in circulation. S-RBD binding IgG was measured using serial dilutions of plasma in an ELISA, and neutralizing antibodies were measured with serial

dilutions of plasma in a microneutralization assay using replication competent SARS-CoV-2 virus (10). Curves were fit to these data, and area under the curve (AUC) values calculated. Anti-S-RBD IgG and neutralization AUC values each varied over a wide range across study subjects (1e2.7-1e4.9 and 1e0.8-1e3.0, respectively). As expected based on prior studies (3, 10), there was a trend toward higher anti-S-RBD IgG and neutralization AUC values in the severe group relative to the mild group, although these differences were not statistically significant, likely due to the small number of subjects (Figure 2A-B). We next evaluated whether there was a correlation between the frequency of S-RBD+ class switched MBC and levels of plasma anti-S-RBD IgG (Figure 2C) or levels of plasma neutralizing antibodies (Figure 2D). Notably, there was a significant correlation across all subjects between frequency of S-RBD+ class switched MBC and levels of plasma anti-S-RBD IgG ($r=0.54$, $p=0.04$). We did not observe a significant correlation between frequency of S-RBD+ class switched MBC and levels of neutralizing antibodies ($r=0.31$, $p=0.28$), possibly because only a subset of S-RBD+ MBC are specific for neutralizing epitopes. The single individual without detectable S-RBD-specific class switched MBC had the lowest levels of plasma anti-S-RBD IgG (AUC=1e2.7) and neutralizing antibodies (AUC=1e0.8) in the study. Overall, these data show that S-RBD-specific class switched MBC were detectable in the circulation of most infected individuals, but that those with lower levels of plasma antibodies also showed lower frequency of S-RBD+ class switched MBC.

UMAP analysis of class switched MBC surface markers.

To further characterize the phenotypes of S-RBD-specific and nonspecific class switched MBC in healthy, mild, or severe COVID-19 patients, we studied surface expression of CD21, CD27, FCRL5, CXCR5, CD22, BTLA, and CD38. For class switched (IgM-, IgD-) MBC, CD21 and CD27 expression allow identification of intermediate MBC (intMBC, CD21+ CD27-), resting

MBC (rMBC, CD21+, CD27+), activated MBC (actMBC, CD21- CD27+), and atypical MBC (atyMBC, CD21- CD27-) subsets. B- and T- lymphocyte attenuator (BTLA) or CD272 and CD22/Siglec2 are immune cell inhibitory receptors with cytoplasmic immunoreceptor tyrosine-based inhibition motifs (ITIMs) (29-32), while FCRL5 has two ITIMs and one immunoreceptor tyrosine-based activation motif (ITAM) (33, 34). CXC chemokine receptor type 5 (CXCR5) is a germinal center homing receptor that is useful, along with other surface markers, for differentiation of double negative 1 (DN1) B cells, which are MBC precursors, from double negative 2 (DN2) B cells, which are extrafollicular ASC precursors (35-37). CD38 expression varies across MBC subsets, and is typically low or negative on actMBC, atyMBC, and DN2 populations.

We first analyzed a UMAP projection of class switched MBC from healthy, mild, and severe groups generated based on binding of S-RBD and expression of CD21, CD27, CD38, CD22, FCRL5, CXCR5, and BTLA (Figure 3A). This UMAP showed a clear segregation of S-RBD+ cells from S-RBD- cells. S-RBD+ cells from severe and mild patients were co-mingled, as were S-RBD- cells from severe, mild, and healthy control groups. From this UMAP clustering projection, we extrapolated multigraph color mapping of the receptors showing a range of expression of all surface markers except BTLA (Figure 3B). CD22 and CD38 expression were greater in the S-RBD+ population than in the S-RBD- cells from COVID-19 patients or healthy donors. Notably, the S-RBD+ population also contained the cells with the highest and lowest levels of FCRL5 expression. To further analyze any differences between expression of these surface markers on all MBC between severe or mild COVID-19 patients and healthy donors, we generated a second UMAP that did not include S-RBD binding as a variable (Supplemental Figure 3). In this UMAP, there was no segregation of cells from severe, mild, or healthy donor

groups, indicating that receptor expression was similar across all three groups. Overall, these UMAPs showed CD22 and CD38 upregulation in S-RBD+ MBC, and a subset of S-RBD+ MBC showed very high expression of FCRL5.

Quantifying subsets of S-RBD nonspecific and S-RBD-specific class switched MBC

To better understand the functional phenotypes of the S-RBD-specific MBC identified in both mild and severe groups, we compared the frequencies of intMBC, rMBC, actMBC, and atyMBC among S-RBD-specific and S-RBD nonspecific class switched MBC at the level of individual participants (Figure 4). Class switched (IgM-, IgD-) MBC subsets identified based on CD21 and CD27 expression have notably different phenotypes (38). Classical MBC, also called rMBC, persist for months to years and respond to antigen re-challenge by proliferating and differentiating into antibody-producing ASC. ActMBC are cells that recently left germinal centers and are already primed to become antibody secreting plasma cells (39). IntMBC likely represent a transitional state between MBC subsets. AtyMBC were recently found to be more frequent among bulk (not antigen specific) MBC during acute SARS-CoV-2 infection (40). AtyMBC are also present at higher frequencies in chronic infections like HIV-1, hepatitis C virus, tuberculosis, or malaria, but their functional significance is unclear (41-43). They often express inhibitory receptors like FCRL4 (44), but they have also been shown to produce protective antibodies during malaria infection (43).

We detected medians of 69.5 absolute S-RBD specific and 13,971 S-RBD nonspecific class switched MBC for each participant (range=1-454 S-RBD specific, 152-84,645 S-RBD nonspecific MBC). Only donors with more than 10 S-RBD specific cells were included in subset

analyses of S-RBD specific MBC, so subject A0046 (no detectable S-RBD-specific class switched MBC frequency above background) and A0077 (severe lymphopenia) were excluded. S-RBD nonspecific MBC were adequately abundant in all participants to allow their inclusion in all analyses. There were no statistically significant differences in the frequencies of intMBC, rMBC, or atyMBC subsets among S-RBD-specific or S-RBD nonspecific class switched MBC from healthy, mild or severe participants (Figure 4). Although overall frequencies of atyMBC did not differ between groups, we observed wide variation in the frequency of atyMBC among S-RBD+ MBC in the severe group. Notably, the two severe subjects with highest atyMBC frequency among S-RBD+ MBC, A0190 and A0224, were also the two subjects who remained intubated at the time of this analysis, whereas the other subjects in the severe group had recovered sufficiently to be discharged from the hospital. The third intubated severe patient, A077, was excluded from this analysis due to lymphopenia. In addition, actMBC were significantly more frequent among both S-RBD nonspecific and S-RBD-specific MBC populations in severe participants compared to healthy and mild participants (e.g. mean frequency of severe S-RBD+ MBC vs. healthy S-RBD- MBC, 16.09% vs. 5.53%, p=0.01) (Figure 4C). This likely represents greater ongoing immune activation in the severe infection group relative to the healthy and mild groups and is also consistent with the observed trend toward higher frequency of ASC in the severe group (Figure 1A). We observed a wide range in the frequency of S-RBD specific actMBC, particularly among severe participants. There were no clear unifying clinical characteristics among the three severe subjects with highest frequencies of actMBC among S-RBD+ MBC (21, 24, and 27%), as their ages ranged from 52 to 76 years, days from onset of symptoms were near the median for the group (39-46 days), and maximum oxygen support ranged from 2L via nasal cannula to intubation.

We were also interested in evaluating the frequency of double negative 1 (DN1) (IgD-, CD27-, CD21+, CXCR5+, FCRL5-) and double negative 2 (DN2) (IgD-, CD27-, CD21-, CXCR5-, FCRL5+) populations among S-RBD+ and S-RBD- B cells from healthy, mild, and severe groups, since since DN1 cells are MBC precursors, and DN2 cells are ASC precursors with an extrafollicular origin that often reach high frequency in the setting of active autoimmune disease (Supplemental Figure 4)(37). We observed no statistically significant differences between class switched DN1 and DN2 frequencies among these different populations, although there was a trend toward greater DN2 frequency in both S-RBD- and S-RBD+ cells from the severe group.

Overall, these data demonstrate an expected distribution of S-RBD-specific cells among MBC subsets, with the largest proportion of S-RBD-specific class switched MBC in both mild and severe groups falling in the rMBC (classical) subset.

Expression of activating or inhibitory surface markers on class switched MBC and MBC subsets.

To further investigate the differential expression of surface markers that we observed in the UMAP projections of grouped samples, we compared expression of FCRL5, CXCR5, CD22, and CD38 at the level of individual participants between healthy, mild S-RBD-, mild S-RBD+, severe S-RBD-, and severe S-RBD+ groups (Figure 5). BTLA expression was not included in this analysis given no differential expression in the UMAP. We found that FCRL5 was dramatically upregulated in mild S-RBD+ MBC relative to healthy cells, mild S-RBD- cells, and severe S-RBD+ cells ($p=<0.0001$, 0.003, and 0.01, respectively). FCRL5 was also upregulated to a lesser, but still significant extent on severe S-RBD+, mild S-RBD-, and severe S-RBD- MBC relative to healthy MBC ($p=0.01$, 0.03, and 0.04, respectively) (Figure 5A). The frequency of CXCR5+ cells among class switched MBC was not significantly different between the groups

(Figure 5B). Since CD22/siglec-2 is ubiquitously expressed on B cells, we analyzed its relative expression by comparing mean fluorescence intensities (MFI). Compared to healthy controls, CD22 was upregulated on mild S-RBD+ class switched MBC ($p=0.04$) (Figure 5C), which was consistent with upregulation of CD22 in the S-RBD+ population in the UMAP analysis. Among class switched MBC, CD38 expression did not differ significantly between SARS-CoV-2 infected and healthy participants (Figure 5D), although there was a trend toward greater expression of CD38 on mild S-RBD+ class switched MBC, which was consistent with upregulation in the S-RBD+ population in the UMAP analysis.

Having observed significant upregulation of both FCRL5 and CD22, and a trend toward upregulation of CD38 on S-RBD+ class switched MBC, we analyzed expression of surface markers on MBC subsets rMBC, intMBC, actMBC, and atyMBC (Figure 6 and Supplemental Figure 5). As with total class switched S-RBD+ MBC, we found that FCRL5 was dramatically upregulated on mild S-RBD+ rMBC relative to healthy rMBC, mild S-RBD- rMBC, and severe S-RBD+ rMBC ($p=<0.0001$, 0.038, and 0.038, respectively). FCRL5 was also upregulated to a lesser, but still significant extent on severe S-RBD+ and mild S-RBD- rMBC relative to healthy rMBC ($p=0.017$ and 0.017, respectively) (Figure 6). As shown in Supplemental Figure 5, CXCR5 was significantly downregulated on mild S-RBD+ atyMBC relative to healthy atyMBC, mild S-RBD- atyMBC, and severe S-RBD+ atyMBC ($p=0.003$, 0.020, and 0.009, respectively). CD22 was significantly upregulated on mild S-RBD+ rMBC and intMBC relative to healthy cells ($p=0.020$ and 0.033, respectively). CD38+ cells were not significantly different between the groups. Taken together, these results indicate that FCRL5 was significantly upregulated on S-RBD-specific rMBC in both mild and severe infection. In mild but not severe infection, CD22

311 was upregulated on S-RBD-specific rMBC and intMBC, and CXCR5 was downregulated on S-
312 RBD-specific atyMBC.

313

Discussion

To investigate the durability of B cell immunity after SARS-CoV-2 infection, we analyzed S-RBD-specific B cells in ambulatory COVID-19 patients with mild disease and hospitalized patients with moderate to severe disease, at a median of 54 days after onset of symptoms. We detected S-RBD-specific class-switched MBC in 13 out of 14 participants, failing only in the individual with lowest plasma levels of anti-S-RBD IgG and neutralizing antibodies. We saw a significant correlation between frequency of S-RBD+ class switched MBC and plasma anti-S-RBD IgG levels across all participants, indicating that individuals with lower plasma antibody titers may also mount less robust anti-S-RBD MBC responses. The largest proportion of S-RBD-specific class-switched MBC in both cohorts were rMBC. AtyMBC were a minor population. FCRL5 was upregulated on S-RBD-specific rMBC after severe infection, and upregulated even more dramatically after mild infection.

These findings are of particular interest given the observation of Kaneko et al. of a dramatic loss of germinal centers in lymph nodes and spleens after SARS-CoV-2 infection (13). This observation would suggest that SARS-CoV-2-specific B cells in infected individuals lack T cell help and would therefore have reduced capacity to undergo class switching and transition to a resting memory phenotype. Our data indicate that despite this loss of germinal centers, T cell help is adequate to facilitate class switching of S-RBD-specific B cells, and transition of many of these cells to a resting state, regardless of disease severity. These data support prior studies, which also found that the majority of S-RBD-specific B cells in individuals who had recovered from COVID-19 showed a resting memory phenotype (45, 46). We did not measure the extent of somatic hypermutation of these B cells, but multiple groups have already demonstrated that

human S-RBD-specific antibodies acquire enough somatic mutations to achieve very high affinity (14-18), again demonstrating that T cell help is adequate in most individuals.

A prior study by Oliviero et al. of bulk (not antigen-specific) MBC subsets during acute or convalescent COVID-19 found that atyMBC were expanded during acute infection, with atyMBC frequencies normalizing during convalescence (40). Our study extends that evaluation by studying both S-RBD-specific and S-RBD nonspecific MBC. We found that S-RBD-specific and S-RBD nonspecific atyMBC, DN1, and DN2 frequencies did not differ significantly from healthy controls, but S-RBD-specific and S-RBD nonspecific actMBC were expanded in severely infected individuals. This observation of increased frequency of actMBC in severe disease might be explained by studies demonstrating greater activation of T cells, including CD4+ T follicular helper cells, in severe COVID-19 disease (47, 48). The contrast of our results with those of Oliviero et al. likely arise from differing timing after infection, and also by our focus on antigen-specific MBC. The fact that frequencies of atyMBC, DN1, and DN2 B cells frequencies do not differ from healthy controls provides further evidence that S-RBD-specific MBC response is probably normally functional.

It is interesting that the single individual without detectable S-RBD-specific class switched MBC was asymptomatic throughout infection, and also had the lowest levels of anti-S-RBD IgG and neutralizing antibodies in the study. Given the low frequency of S-RBD specific MBC across the cohort, we would need to analyze a larger number of PBMC to confirm with confidence that this individual is truly negative for S-RBD-specific class switched MBC. We also saw a significant correlation between frequency of S-RBD+ class switched MBC and plasma anti-S-RBD IgG levels across all participants, indicating that individuals with relatively lower plasma antibody titers may also mount relatively less robust anti-S-RBD MBC responses.

A limitation of this study is the lack of long-term longitudinal sampling of B cells after infection, which would be required to prove that the S-RBD-specific MBC responses observed here are truly durable. These studies will be pursued as longitudinal samples become available. Additionally, we analyzed low numbers of S-RBD specific class-switched MBC in some subjects due to low frequency and a limitation of available PBMCs, so phenotyping of MBC subsets should be interpreted with some caution. However, we have shown here that S-RBD-specific MBC in most infected individuals have a phenotype that very closely resembles the phenotype of germinal center-derived MBC induced by effective vaccination against influenza and tetanus. Indeed, this observation is supported by two very recent studies with longitudinal B cell sampling after COVID-19 infection, demonstrating that S-RBD-specific B cell frequencies were stable or increasing over time (46, 49).

Of particular note in this study is the upregulation of FCRL5 on S-RBD-specific class switched rMBC after either mild or severe disease. FCRL5 is expressed by most germinal center-derived MBC in plasmodium-infected mice, and these FCRL5+ MBC differentiate into ASC on re-challenge (25). In addition, Kim et al. found that in humans, presumably vaccinated against tetanus months to years prior, FCRL5 was upregulated on tetanus specific rMBC (CD21+, CD27+) but not on bulk rMBC (25). Nellore et al. showed similar results after influenza vaccination of humans, demonstrating that hemagglutinin (HA)-specific, FCRL5+ MBC were induced by vaccination, and that these FCRL5+ MBC preferentially differentiated into plasmablasts upon antigen rechallenge approximately a year after vaccination (26). Although FCRL5 was upregulated on S-RBD specific rMBC in both mild and severe disease, it was upregulated to a greater extent in mild disease. This may reflect a more typical MBC response in mild disease, and a more dysfunctional response in severe disease. Further longitudinal studies

are needed to compare persistence and expansion after antigen re-challenge of rMBC with very high vs more modest FCRL5 expression. Further studies will be also be necessary to understand the implications of CD22 upregulation on S-RBD-specific rMBC and intMBC, CXCR5 downregulation on S-RBD-specific atyMBC, and a trend toward CD38 upregulation on S-RBD-specific rMBC and actMBC. The functions of CXCR5 and CD38 in this context are unclear, but we would speculate that since CD22 is an inhibitory receptor, expression may help to maintain MBC in a resting state, which could favor long-term persistence of S-RBD-specific MBC. Overall, despite our lack of longitudinal testing, the phenotypic similarity of S-RBD-specific MBC in this study to typical, germinal center-derived MBC induced by effective vaccination provide strong evidence that these S-RBD-specific MBC are durable and functional.

In summary, we have demonstrated that S-RBD-specific class-switched MBC develop in most SARS-CoV-2-infected individuals, including those with mild disease or low levels of plasma anti-S-RBD IgG and neutralizing antibodies. The most abundant subset of S-RBD-specific class-switched MBC in both cohorts were rMBC, and atyMBC were a minor population. FCRL5, a marker of a functional memory response when expressed on antigen-specific rMBC, was dramatically upregulated on S-RBD-specific rMBC, particularly after mild infection. These data indicate that most SARS-CoV-2-infected individuals develop S-RBD-specific, class-switched MBC that phenotypically resemble B cells induced by effective vaccination against other pathogens, providing evidence for durable humoral immunity against SARS-CoV-2 after recovery from either mild or severe COVID-19 disease. These data have implications for risk of reinfection after recovery from COVID-19, and also provide a standard against which B cell responses to novel SARS-CoV-2 vaccines could be compared.

Methods

Study participants

Participants with mild COVID-19 disease who never required hospitalization or supplemental oxygen were identified in a cohort of ambulatory COVID-19 patients. Symptoms in this cohort were tracked using a FLU-PRO score calculated from a participant survey, as previously described (27). Participants with moderate to severe COVID-19 disease were selected from a cohort of hospitalized patients (28), matched with the mild participants based on time since onset of symptoms at the time of blood sampling. PBMC cryopreserved prior to the onset of the COVID-19 pandemic were also obtained from anonymous healthy blood donors. Healthy and COVID-19 participant blood specimens were ficoll gradient separated into plasma and PBMCs. PBMCs were viably cryopreserved in FBS + 10% DMSO for future use.

Expression and purification of soluble Spike protein Receptor Binding Domain (S-RBD)

Plasmid preparation

Recombinant plasmid constructs containing modified S protein Receptor Binding Domain (S-RBD) and a beta-lactamase (amp) gene were obtained (Stadlbauer 2020) and amplified in E.coli after transformation and growth on LB agar plates coated with Ampicillin. The plasmids were extracted using GigaPrep kits (Thermo Fisher Scientific) and eluted in molecular biology grade water.

Recombinant protein expression

HEK293.2sus cells (ATCC) were obtained and adapted to Freestyle™ F-17 medium (Thermo Fisher Scientific) and BalanCD® (Irvine Scientific) using polycarbonate shake flasks

(Fisherbrand) with 4mM GlutaMAX supplementation (Thermo Fisher Scientific). The cells were routinely maintained every 4 days at a seeding density of 0.5 million cells/mL. They were cultured at 37°C, 90% humidity with 5% CO2 for cells in BalanCD® while those in F-17 were maintained at 8% CO2. Cells were counted using trypan blue dye (Gibco) exclusion method and a hemocytometer. Cell viability was always maintained above 90%. Twenty-four hours prior to transfection (Day -1), the cells were seeded at a density of 1 million cells/mL, ensuring that the cell viability was above 90%. Polyethylenimine (PEI) stocks, with 25 kDa molecular mass (Polysciences), were prepared in MilliQ water at a concentration of 1 mg/mL. This was filter sterilized through a 0.22 μm syringe filter (Corning), aliquoted and stored at -20°C. On the day of transfection (Day 0), the cells were counted to ensure sufficient growth and viability. OptiPRO™ SFM (Gibco) was used as the medium for transfection mixture. For 100 mL of cell culture, 2 tubes were aliquoted with 6.7 mL each of OptiPRO™, one for PEI and the other for rDNA. DNA:PEI ratio of 1:3.5 was used for transfection. A volume of 350 μL of prepared PEI stock solution was added to tube 1 while 100 μg of rDNA was added to tube 2 and incubated for 5 minutes. Post incubation, these were mixed together, incubated for 10 minutes at RT and then added to the culture through gravity addition. The cells were returned back to the 37°C incubator. A day after transfection (Day 1), the cells were spun down at 1,000 rpm for 7 minutes at RT and resuspended in fresh media with GlutaMAX™ supplementation. 3-5 hours after resuspension, 0.22 μm sterile filtered Sodium butyrate (EMD Millipore) was added to the flask at a final concentration of 5 mM (Grünberg et al.). The cells were allowed to grow for a period of 4-5 days. Cell counts, viability, glucose and lactate values were measured every day. Cells were harvested when either the viability fell below 60% or when the glucose was depleted, by centrifugation at 5000 rpm for 10 minutes at RT. Cell culture supernatants containing either

recombinant S-RBD or S protein were filtered through 0.22 μm PES membrane stericup filters (Millipore Sigma) to remove cell debris and stored at -20°C until purification.

Protein purification

Protein purification by immobilized metal affinity chromatography (IMAC) and gravity flow was adapted from previous methods (23). After washing with Phosphate-Buffered Saline (PBS; Thermo Fisher Scientific), Nickel-Nitrilotriacetic acid (Ni-NTA) agarose (Qiagen) was added to culture supernatant followed by overnight incubation (12-16 hours) at 4 °C on a rotator. For every 150 mL of culture supernatant, 2.5 mL of Ni-NTA agarose was added. 5mL gravity flow polypropylene columns (Qiagen) were equilibrated with PBS. One polypropylene column was used for every 150 mL of culture supernatant. The supernatant-agarose mixture was then loaded onto the column to retain the agarose beads with recombinant proteins bound to the beads. Each column was then washed, first with 1X culture supernatant volume of PBS and then with 25 mL of 20 mM imidazole (Millipore Sigma) in PBS wash buffer to remove host cell proteins. Recombinant proteins were then eluted from each column in three fractions with 5 mL of 250 mM imidazole in PBS elution buffer per fraction giving a total of 15 mL eluate per column. The eluate was subsequently dialyzed several times against PBS using Amicon Ultra Centrifugal Filters (Millipore Sigma) at 7000 rpm for 20 minutes at 10 °C to remove the imidazole and concentrate the eluate. Filters with a 10 kDa molecular weight cut-off were used for S-RBD eluate. The final concentration of the recombinant S-RBD and S proteins was measured by bicinchoninic acid (BCA) assay (Thermo Fisher Scientific), and purity was assessed on 10% SDS-PAGE (Bio-Rad) followed by Coomassie blue staining. After sufficient destaining in water overnight, clear single bands were visible for S-RBD.

Viruses and cells.

Vero-E6 cells (ATCC CRL-1586) and Vero-E6-TMPRSS2 cells (24) were cultured in Dulbecco's modified Eagle medium (DMEMD) containing 10% fetal bovine serum (Gibco), 1 mM glutamine (Invitrogen), 1 mM sodium pyruvate (Invitrogen), 100 U/ml of penicillin (Invitrogen), and 100 µg/ml of streptomycin (Invitrogen) (complete media or CM). Cells were incubated in a 5% CO2 humidified incubator at 37°C. The SARS-CoV-2/USA-WA1/2020 virus was obtained from BEI Resources. The infectious virus titer was determined on Vero cells using a 50% tissue culture infectious dose (TCID50) assay as previously described for SARS-CoV (25, 26). Serial 10-fold dilutions of the virus stock were made in infection media (IM, which is identical to CM except the FBS is reduced to 2.5%), then then 100 µl of each dilution was added to Vero cells in a 96-well plate in sextuplicate. The cells were incubated at 37°C for 4 days, visualized by staining with naphthol blue-black, and scored visually for cytopathic effect. A Reed and Muench calculation was used to determine TCID50 per ml (27).

Measurement of endpoint anti-S-RBD IgG titer.

The protocol was adapted from a published protocol from Dr. Florian Krammer's laboratory (Stadlbauer 2020). Ninety-six well plates (Immulon 4HBX, Thermo Fisher) were coated with S-RBD at a volume of 50 µl of 2 µg/ml of diluted antigen in filtered, sterile 1xPBS (Thermo Fisher) at 4°C overnight. Coating buffer was removed, plates were washed three times with 300 µl of PBS-T wash buffer (1xPBS plus 0.1% Tween 20, Fisher Scientific), and blocked with 200 µl of PBS-T with 3% non-fat milk (milk powder, American Bio) by volume for one hour at room temperature. All plasma samples were heat inactivated at 56°C on a heating block for one hour prior to use. Negative control samples were prepared at 1:10 dilutions in PBS-T in 1% non-fat milk and plated at a final concentration of 1:100. A monoclonal antibody (mAb) specific for the

SARS-CoV-2 spike protein was used as a positive control (1:5,000, Sino Biological). For serial dilutions of plasma on S-RBD coated plates, plasma samples were prepared in three-fold serial dilutions starting at 1:20 in PBST in 1% non-fat-milk. Blocking solution was removed and 10 µl of diluted plasma was added in duplicates to plates and incubated at room temperature for two hours. Plates were washed three times with PBS-T wash buffer and 50 µl secondary antibody was added to plates and incubated at room temperature for one hour. Anti-human secondary antibodies used included Fc-specific total IgG HRP (1:5,000 dilution, Invitrogen), prepared in PBS-T plus 1% non-fat milk. Plates were washed and all residual liquid removed before adding 100 µl of SIGMAFAST OPD (o-phenylenediamine dihydrochloride) solution (Sigma Aldrich) to each well, followed by incubation in darkness at room temperature for ten minutes. To stop the reaction, 50 µl of 3M hydrochloric acid (HCl, Fisher Scientific) was added to each well. The OD of each plate was read at 490nm (OD490) on a SpectraMax i3 ELISA plate reader (BioTek). The positive cutoff value for each plate was calculated by summing the average of the negative values and three times the standard deviation of the negatives. All values at or above the cutoff value were considered positive. Values were graphed on a dose response curve, a best fit line drawn by nonlinear regression, and area under the curve (AUC) calculated.

Measurement of endpoint neutralization titer.

Plasma neutralization titers were determined as described for SARS-CoV (Schaecher 2008). Two-fold dilutions of plasma (starting at a 1:20 dilution) were made in IM. Infectious virus was added to the plasma dilutions at a final concentration of 1x104 TCID50/ml (100 TCID50 per 100ul). The samples were incubated for one hour at room temperature, then 100 uL of each dilution was added to one well of a 96 well plate of VeroE6-TMPRSS2 cells in sextuplet for 6 hours at 37°C. The inoculums were removed, fresh IM was added, and the plates were incubated

at 37°C for 2 days. The cells were fixed by the addition of 150 uL of 4% formaldehyde per well, incubated for at least 4 hours at room temperature, then stained with Napthol blue black. The nAb titer was calculated as the highest serum dilution that eliminated cytopathic effect (CPE) in 50% of the wells. Values were graphed on a dose response curve, a best fit line drawn by nonlinear regression, and area under the curve (AUC) calculated.

Cell staining and flow cytometry

PBMCs were isolated from blood using ficoll separation gradient and viably frozen. Cells were thawed before use, and 5e6-10e6 PBMCs were stained from each participant. Fc blocker (BD Cat #564220) diluted in FACS Buffer (1x PBS with 1% BSA) was added to the cells and incubated for 30minutes on ice or 4c. The cells were then washed twice with FACS buffer. Soluble 6x-His tagged S-RBD protein was then added to the cells and incubated at room temperature for 30 min. This was followed by wash steps with FACS buffer. Conjugated antibodies (Suppl. Table 1 for list of antibodies and their conjugate fluorophores) and live dead stain was then added to the cells and incubated for an additional 30min. The cells were washed two or three more times before running the cells on BD Biosciences LSR II instrument. 1e6-6e6 total events were collected for each participant, resulting in medians of 69.5 absolute S-RBD+ and 13,971 S-RBD- class switched MBC for each participant (range=1-454 S-RBD+, 152-84,645 S-RBD- MBC). All S-RBD+ MBC from all study subjects (n=1600) were included in each UMAP. To allow clear visualization of both S-RBD+ and S-RBD- cells in the Figure 3 UMAP, S-RBD- cells were downsampled for each subject to match the number of S-RBD+ cells from that subject. For Supplemental Figure 3, S-RBD- cells were downsampled to 3000 cells per subject to maximize the number of cells analyzed while equalizing the input from each subject. The subject with only 1 S-RBD+ cell was excluded from S-RBD+ MBC subset analyses.

Positive gates for each fluorophore were set after compensation and using fluorescence minus one (FMO) staining and isotype control antibodies. Representative FCRL5 staining is shown in Supplemental Figure 6.

Confirmation of specificity of S-RBD staining.

For double staining with two different S-RBD proteins (Supplemental Figure 2), a similar staining protocol was used with the inclusion of S-RBD, Mouse IgG1 Fc,Avitag™ (MALS verified) protein from AcroBiosystems (Fisher Scientific Catalog No. 50-201-9394). Binding of this protein was detected with PE anti-mouse IgG1 Antibody (Supplemental Table 1). BTLA, CD22, FCRL5, and CXCR5 were not stained in this experiment.

Statistical analysis

FlowJo software was used to analyze all the flow results from the LSRII. Statistical analyses were performed in Prism (Graphpad software). Two group comparisons were performed with two-sided t tests if data were normally distributed based on Shapiro Wilk normality test or Mann Whitney rank test if data were not normally distributed. Multi-group comparisons were performed using one-way ANOVA if data were normally distributed based on Shapiro Wilk normality test or Kruskal-Wallis test if data were not normally distributed, with p values adjusted for multiple comparisons using the Benjamini, Krieger and Yekutieli method. Adjusted p values < 0.05 were considered significant.

Study approval.

This research was approved by the Johns Hopkins University School of Medicine's Institutional Review Board (IRB). Prior to blood collection, all participants provided informed written consent.

Author Contributions. COO conceived the project, performed experiments, interpreted data, and wrote the initial manuscript draft; NES conceived the project, performed experiments, and interpreted data; PWB interpreted data; HSP, KL, AG, and SD performed experiments and interpreted data; AA interpreted data; SCR interpreted data; PL and MJB provided reagents. AP performed experiments and interpreted data; SLK performed experiments and interpreted data; YCM conceived the project and provided participant samples; ALC conceived the project, provided participant samples, and interpreted data; JRB conceived the project, interpreted data, and wrote the initial manuscript draft. All authors reviewed and edited the manuscript.

Acknowledgements. We would like to thank participants in the study, Florian Krammer for providing the S-RBD plasmid, and members of the Johns Hopkins Viral Hepatitis Center for thoughtful discussion. We thank the Bloomberg Flow Cytometry and Immunology Core for equipment and technical assistance. We thank the National Institute of Infectious Diseases, Japan, for providing VeroE6TMPRSS2 cells and acknowledge the Centers for Disease Control and Prevention, BEI Resources, NIAID, NIH for SARS-related coronavirus 2, isolate USA-WA1/2020, NR-5228.This research was supported by the National Institutes of Health grants R01AI127469 and R21AI151353 (to J.R.B.), U54CA260492 (SLK and AC), and in part by the NIH Center of Excellence for Influenza Research and Surveillance (HHSN272201400007C, to AP and SLK).

References

1. Guan WJ, and Zhong NS. Clinical Characteristics of Covid-19 in China. Reply. *N Engl J Med.* 2020;382(19):1861-2.
2. Wang Z, Yang B, Li Q, Wen L, and Zhang R. Clinical Features of 69 Cases With Coronavirus Disease 2019 in Wuhan, China. *Clin Infect Dis.* 2020;71(15):769-77.
3. Long QX, Liu BZ, Deng HJ, Wu GC, Deng K, Chen YK, Liao P, Qiu JF, Lin Y, Cai XF, et al. Antibody responses to SARS-CoV-2 in patients with COVID-19. *Nat Med.* 2020.
4. Seow J, Graham C, Merrick B, Acors S, Steel KJA, Hemmings O, O'Bryne A, Kouphou N, Pickering S, Galao R, et al. Longitudinal evaluation and decline of antibody responses in SARS-CoV-2 infection. *medRxiv.* 2020:2020.07.09.20148429.
5. Ibarrondo FJ, Fulcher JA, Goodman-Meza D, Elliott J, Hofmann C, Hausner MA, Ferbas KG, Tobin NH, Aldrovandi GM, and Yang OO. Rapid Decay of Anti-SARS-CoV-2 Antibodies in Persons with Mild Covid-19. *N Engl J Med.* 2020;383(11):1085-7.
6. Patel MM, Thornburg NJ, Stubblefield WB, Talbot HK, Coughlin MM, Feldstein LR, and Self WH. Change in Antibodies to SARS-CoV-2 Over 60 Days Among Health Care Personnel in Nashville, Tennessee. *JAMA.* 2020.
7. Wajnberg A, Amanat F, Firpo A, Altman D, Bailey M, Mansour M, McMahon M, Meade P, Mendu DR, Muellers K, et al. SARS-CoV-2 infection induces robust, neutralizing antibody responses that are stable for at least three months. *medRxiv.* 2020:2020.07.14.20151126.
8. Isho B, Abe KT, Zuo M, Jamal AJ, Rathod B, Wang JH, Li Z, Chao G, Rojas OL, Bang YM, et al. Persistence of serum and saliva antibody responses to SARS-CoV-2 spike antigens in COVID-19 patients. *Sci Immunol.* 2020;5(52).
9. Iyer AS, Jones FK, Nodoushani A, Kelly M, Becker M, Slater D, Mills R, Teng E, Kamruzzaman M, Garcia-Beltran WF, et al. Persistence and decay of human antibody responses to the receptor binding domain of SARS-CoV-2 spike protein in COVID-19 patients. *Sci Immunol.* 2020;5(52).
10. Klein SL, Pekosz A, Park HS, Ursin RL, Shapiro JR, Benner SE, Littlefield K, Kumar S, Naik HM, Betenbaugh MJ, et al. Sex, age, and hospitalization drive antibody responses in a COVID-19 convalescent plasma donor population. *J Clin Invest.* 2020.
11. Salimzadeh L, Le Bert N, Dutertre CA, Gill US, Newell EW, Frey C, Hung M, Novikov N, Fletcher S, Kennedy PT, et al. PD-1 blockade partially recovers dysfunctional virus-specific B cells in chronic hepatitis B infection. *J Clin Invest.* 2018;128(10):4573-87.
12. Middleman AB, Baker CJ, Kozinetz CA, Kamili S, Nguyen C, Hu DJ, and Spradling PR. Duration of protection after infant hepatitis B vaccination series. *Pediatrics.* 2014;133(6):e1500-7.
13. Kaneko N, Kuo HH, Boucau J, Farmer JR, Allard-Chamard H, Mahajan VS, Piechocka-Trocha A, Lefteri K, Osborn M, Bals J, et al. Loss of Bcl-6-Expressing T Follicular Helper Cells and Germinal Centers in COVID-19. *Cell.* 2020;183(1):143-57 e13.
14. Robbiani DF, Gaebler C, Muecksch F, Lorenzi JCC, Wang Z, Cho A, Agudelo M, Barnes CO, Gazumyan A, Finkin S, et al. Convergent antibody responses to SARS-CoV-2 in convalescent individuals. *Nature.* 2020;584(7821):437-42.
15. Zost SJ, Gilchuk P, Case JB, Binshtein E, Chen RE, Nkolola JP, Schafer A, Reidy JX, Trivette A, Nargi RS, et al. Potently neutralizing and protective human antibodies against SARS-CoV-2. *Nature.* 2020;584(7821):443-9.
16. Noy-Porat T, Makdasi E, Alcalay R, Mechaly A, Levy Y, Bercovich-Kinori A, Zauberman A, Tamir H, Yahalom-Ronen Y, Israeli M, et al. A panel of human neutralizing mAbs targeting SARS-CoV-2 spike at multiple epitopes. *Nat Commun.* 2020;11(1):4303.

17. Rogers TF, Zhao F, Huang D, Beutler N, Burns A, He WT, Limbo O, Smith C, Song G, Woehl J, et al. Isolation of potent SARS-CoV-2 neutralizing antibodies and protection from disease in a small animal model. *Science.* 2020;369(6506):956-63.
18. Brouwer PJM, Caniels TG, van der Straten K, Snitselaar JL, Aldon Y, Bangaru S, Torres JL, Okba NMA, Claireaux M, Kerster G, et al. Potent neutralizing antibodies from COVID-19 patients define multiple targets of vulnerability. *Science.* 2020;369(6504):643-50.
19. Buchholz UJ, Bukreyev A, Yang L, Lamirande EW, Murphy BR, Subbarao K, and Collins PL. Contributions of the structural proteins of severe acute respiratory syndrome coronavirus to protective immunity. *Proc Natl Acad Sci U S A.* 2004;101(26):9804-9.
20. Du L, He Y, Zhou Y, Liu S, Zheng BJ, and Jiang S. The spike protein of SARS-CoV--a target for vaccine and therapeutic development. *Nat Rev Microbiol.* 2009;7(3):226-36.
21. Li T, Xie J, He Y, Fan H, Baril L, Qiu Z, Han Y, Xu W, Zhang W, You H, et al. Long-term persistence of robust antibody and cytotoxic T cell responses in recovered patients infected with SARS coronavirus. *PLoS One.* 2006;1(e24.
22. Huang AT, Garcia-Carreras B, Hitchings MDT, Yang B, Katzelnick L, Rattigan SM, Borgert B, Moreno C, Solomon BD, Rodriguez-Barraquer I, et al. A systematic review of antibody mediated immunity to coronaviruses: antibody kinetics, correlates of protection, and association of antibody responses with severity of disease. *medRxiv.* 2020:2020.04.14.20065771.
23. Deng W, Bao L, Liu J, Xiao C, Liu J, Xue J, Lv Q, Qi F, Gao H, Yu P, et al. Primary exposure to SARS-CoV-2 protects against reinfection in rhesus macaques. *Science.* 2020;369(6505):818-23.
24. Chandrashekar A, Liu J, Martinot AJ, McMahan K, Mercado NB, Peter L, Tostanoski LH, Yu J, Maliga Z, Nekorchuk M, et al. SARS-CoV-2 infection protects against rechallenge in rhesus macaques. *Science.* 2020;369(6505):812-7.
25. Kim CC, Baccarella AM, Bayat A, Pepper M, and Fontana MF. FCRL5(+) Memory B Cells Exhibit Robust Recall Responses. *Cell Rep.* 2019;27(5):1446-60 e4.
26. Nellore A, Scharer CD, King RG, Tipton CM, Zumaquero E, Fucile C, Mousseau B, Bradley JE, Macon K, Mi T, et al. Fcrl5 and T-bet define influenza-specific memory B cells that predict long-lived antibody responses. *bioRxiv.* 2019:643973.
27. Blair PW, Brown DM, Jang M, Antar AA, Keruly JC, Bachu V, Townsend JL, Tornheim JA, Keller SC, Sauer L, et al. The clinical course of COVID-19 in the outpatient setting: a prospective cohort study. *medRxiv.* 2020:2020.09.01.20184937.
28. Thompson EA, Cascino K, Ordonez AA, Zhou W, Vaghasia A, Hamacher-Brady A, Brady NR, Sun I-H, Wang R, Rosenberg AZ, et al. Metabolic programs define dysfunctional immune responses in severe COVID-19 patients. *medRxiv.* 2020:2020.09.10.20186064.
29. Crocker PR, Paulson JC, and Varki A. Siglecs and their roles in the immune system. *Nature Reviews Immunology.* 2007;7(4):255-66.
30. Macauley MS, Crocker PR, and Paulson JC. Siglec-mediated regulation of immune cell function in disease. *Nature Reviews Immunology.* 2014;14(10):653-66.
31. Tateno H, Li H, Schur MJ, Bovin N, Crocker PR, Wakarchuk WW, and Paulson JC. Distinct endocytic mechanisms of CD22 (Siglec-2) and Siglec-F reflect roles in cell signaling and innate immunity. *Mol Cell Biol.* 2007;27(16):5699-710.
32. Watanabe N, Gavrieli M, Sedy JR, Yang J, Fallarino F, Loftin SK, Hurchla MA, Zimmerman N, Sim J, Zang X, et al. BTLA is a lymphocyte inhibitory receptor with similarities to CTLA-4 and PD-1. *NatImmunol.* 2003;4(670-9.
33. Davis RS. FCRL regulation in innate-like B cells. *Ann N Y Acad Sci.* 2015;1362(1):110-6.
34. Liao HX, Lynch R, Zhou T, Gao F, Alam SM, Boyd SD, Fire AZ, Roskin KM, Schramm CA, Zhang Z, et al. Co-evolution of a broadly neutralizing HIV-1 antibody and founder virus. *Nature.* 2013;496(7446):469-76.

35. Hardtke S, Ohl L, and Förster R. Balanced expression of CXCR5 and CCR7 on follicular T helper cells determines their transient positioning to lymph node follicles and is essential for efficient B-cell help. *Blood.* 2005;106(6):1924-31.
36. Junt T, Fink K, Förster R, Senn B, Lipp M, Muramatsu M, Zinkernagel RM, Ludewig B, and Hengartner H. CXCR5-Dependent Seeding of Follicular Niches by B and Th Cells Augments Antiviral B Cell Responses. *The Journal of Immunology.* 2005;175(11):7109-16.
37. Sanz I, Wei C, Jenks SA, Cashman KS, Tipton C, Woodruff MC, Hom J, and Lee FE. Challenges and Opportunities for Consistent Classification of Human B Cell and Plasma Cell Populations. *Front Immunol.* 2019;10(2458.
38. Sanz I, Wei C, Lee FE, and Anolik J. Phenotypic and functional heterogeneity of human memory B cells. *Semin Immunol.* 2008;20(1):67-82.
39. Lau D, Lan LY, Andrews SF, Henry C, Rojas KT, Neu KE, Huang M, Huang Y, DeKosky B, Palm AE, et al. Low CD21 expression defines a population of recent germinal center graduates primed for plasma cell differentiation. *Sci Immunol.* 2017;2(7).
40. Oliviero B, Varchetta S, Mele D, Mantovani S, Cerino A, Perotti CG, Ludovisi S, and Mondelli MU. Expansion of atypical memory B cells is a prominent feature of COVID-19. *Cell Mol Immunol.* 2020;17(10):1101-3.
41. Moir S, Ho J, Malaspina A, Wang W, DiPoto AC, O'Shea MA, Roby G, Kottilil S, Arthos J, Proschan MA, et al. Evidence for HIV-associated B cell exhaustion in a dysfunctional memory B cell compartment in HIV-infected viremic individuals. *J Exp Med.* 2008;205(8):1797-805.
42. Joosten SA, van Meijgaarden KE, Del Nonno F, Baiocchini A, Petrone L, Vanini V, Smits HH, Palmieri F, Goletti D, and Ottenhoff TH. Patients with Tuberculosis Have a Dysfunctional Circulating B-Cell Compartment, Which Normalizes following Successful Treatment. *PLoS Pathog.* 2016;12(6):e1005687.
43. Muellenbeck MF, Ueberheide B, Amulic B, Epp A, Fenyo D, Busse CE, Esen M, Theisen M, Mordmuller B, and Wardemann H. Atypical and classical memory B cells produce Plasmodium falciparum neutralizing antibodies. *J Exp Med.* 2013;210(2):389-99.
44. Sohn HW, Krueger PD, Davis RS, and Pierce SK. FcRL4 acts as an adaptive to innate molecular switch dampening BCR signaling and enhancing TLR signaling. *Blood.* 2011;118(24):6332-41.
45. Juno JA, Tan HX, Lee WS, Reynaldi A, Kelly HG, Wragg K, Esterbauer R, Kent HE, Batten CJ, Mordant FL, et al. Humoral and circulating follicular helper T cell responses in recovered patients with COVID-19. *Nat Med.* 2020;26(9):1428-34.
46. Rodda LB, Netland J, Shehata L, Pruner KB, Morawski PA, Thouvenel CD, Takehara KK, Eggenberger J, Hemann EA, Waterman HR, et al. Functional SARS-CoV-2-Specific Immune Memory Persists after Mild COVID-19. *Cell.* 2020.
47. Kuri-Cervantes L, Pampena MB, Meng W, Rosenfeld AM, Ittner CAG, Weisman AR, Agyekum RS, Mathew D, Baxter AE, Vella LA, et al. Comprehensive mapping of immune perturbations associated with severe COVID-19. *Sci Immunol.* 2020;5(49).
48. Chen Z, and John Wherry E. T cell responses in patients with COVID-19. *Nat Rev Immunol.* 2020;20(9):529-36.
49. Dan JM, Mateus J, Kato Y, Hastie KM, Yu ED, Faliti CE, Grifoni A, Ramirez SI, Haupt S, Frazier A, et al. Immunological memory to SARS-CoV-2 assessed for up to 8 months after infection. *Science.* 2021.

Table 1. Participant characteristics

Participant ID	Age	Sex	Race	Ethnicity	Days from symptom onset	FLU-PRO[1]	Supp. O_2[2]
Mild-ambulatory							
SE-JH-A-A0006	63	F	White	Non-Hispanic	63	0.38	none
SE-JH-A-A0021	53	F	Hawaiian/Pacific Islander	Non-Hispanic	68	0.28	none
SE-JH-A-A0033	62	F	White	Hispanic	59	0.19	none
SE-JH-A-A0039	71	F	White	Non-Hispanic	64	0.06	none
SE-JH-A-A0046	56	M	White	Non-Hispanic	46	0	none
SE-JH-A-A0054	43	M	Black	Non-Hispanic	61	0.03	none
SE-JH-A-A0060	32	M	American Indian/ Alaska Native	Non-Hispanic	45	0.09	none
median	*56*				*61*	*0.09*	
Severe-hospitalized							
SE-JH-H-A0006	67	F	Black	Non-Hispanic	90	n/a	4LNC
SE-JH-H-A0026	50	M	Black	Non-Hispanic	104	n/a	HFNC
SE-JH-H-A0077	57	M	White	Non-Hispanic	48	n/a	Intubated
SE-JH-H-A0169	52	M	Other	Non-Hispanic	46	n/a	2LNC
SE-JH-H-A0190	76	F	Black	Non-Hispanic	39	n/a	Intubated
SE-JH-H-A0207	52	M	Black	Non-Hispanic	42	n/a	HFNC
SE-JH-H-A0224	73	M	Other	Non-Hispanic	41	n/a	Intubated
median	*57*				*46*		

[1]Peak FLU-PRO score. [2]Maximum oxygen support required. 4LNC, 4 liters via nasal cannula; HFNC, high flow oxygen via nasal cannula; intubated, requiring mechanical ventilation; 2LNC, 2 liters via nasal cannula.

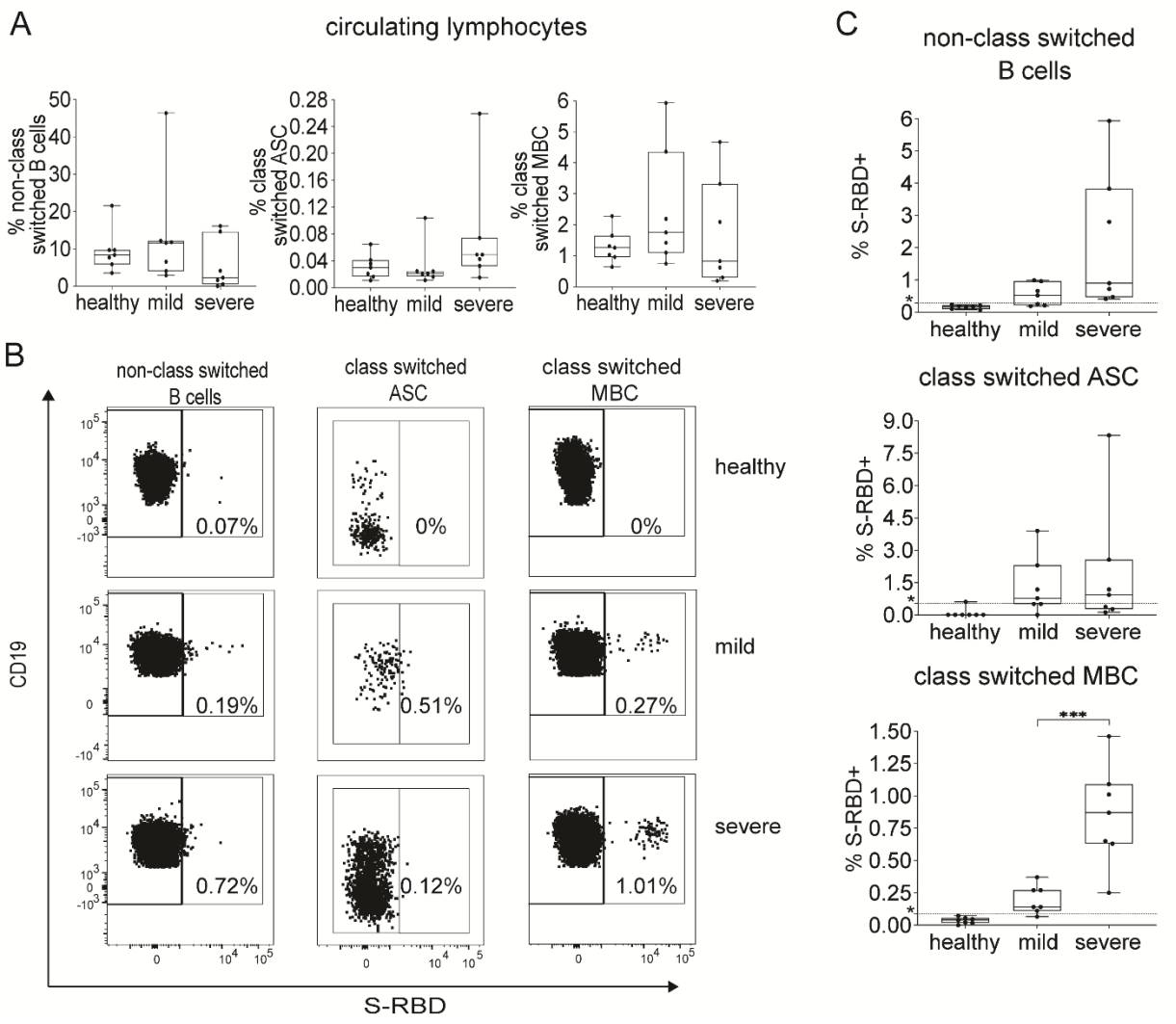

Figure 1. Quantifying S-RBD specific B cells. (A) % of lymphocytes that are class switched MBC, class switched ASC, or non-class switched B cells in healthy (COVID-19 negative), mild (COVID-19+, ambulatory), and severe (COVID-19+, hospitalized) participants (N=7 for each group). **(B)** Gating strategy for S-RBD specific non-class switched B cells (CD3-, CD19+, IgD/IgM+, S-RBD+), S-RBD specific class switched MBC (CD3-, CD19+, IgM-, IgD-, CD38+/- (excluding ++), CD138-, S-RBD+), and S-RBD specific class switched ASC (CD3-, CD19+/-, IgM-, IgD-, CD38++, CD27+, S-RBD+) in healthy, mild, and severe participants. **(C)** % of class switched MBC, class switched ASC, and non-class switched B cells that are S-RBD

specific in healthy, mild, and severe participants (N=7 for each group). Dotted line represents the true positive threshold, defined as the mean plus two standard deviations of the healthy group. For box plots, horizontal lines indicate means, boxes are inter-quartile range, and whiskers are minimum to maximum. Normality of data was determined using Shapiro Wilk normality test. Comparisons in **A** were performed using one-way ANOVA for normally distributed data or Kruskal-Wallis test for non-normally distributed data, with p values adjusted for multiple comparisons using the Benjamini, Krieger and Yekutieli method. Comparisons between mild and severe in **C** were performed with t tests if data were normally distributed or Mann Whitney test if data were not normally distributed. Statistically significant comparisons are indicated (*** $P \leq 0.001$)

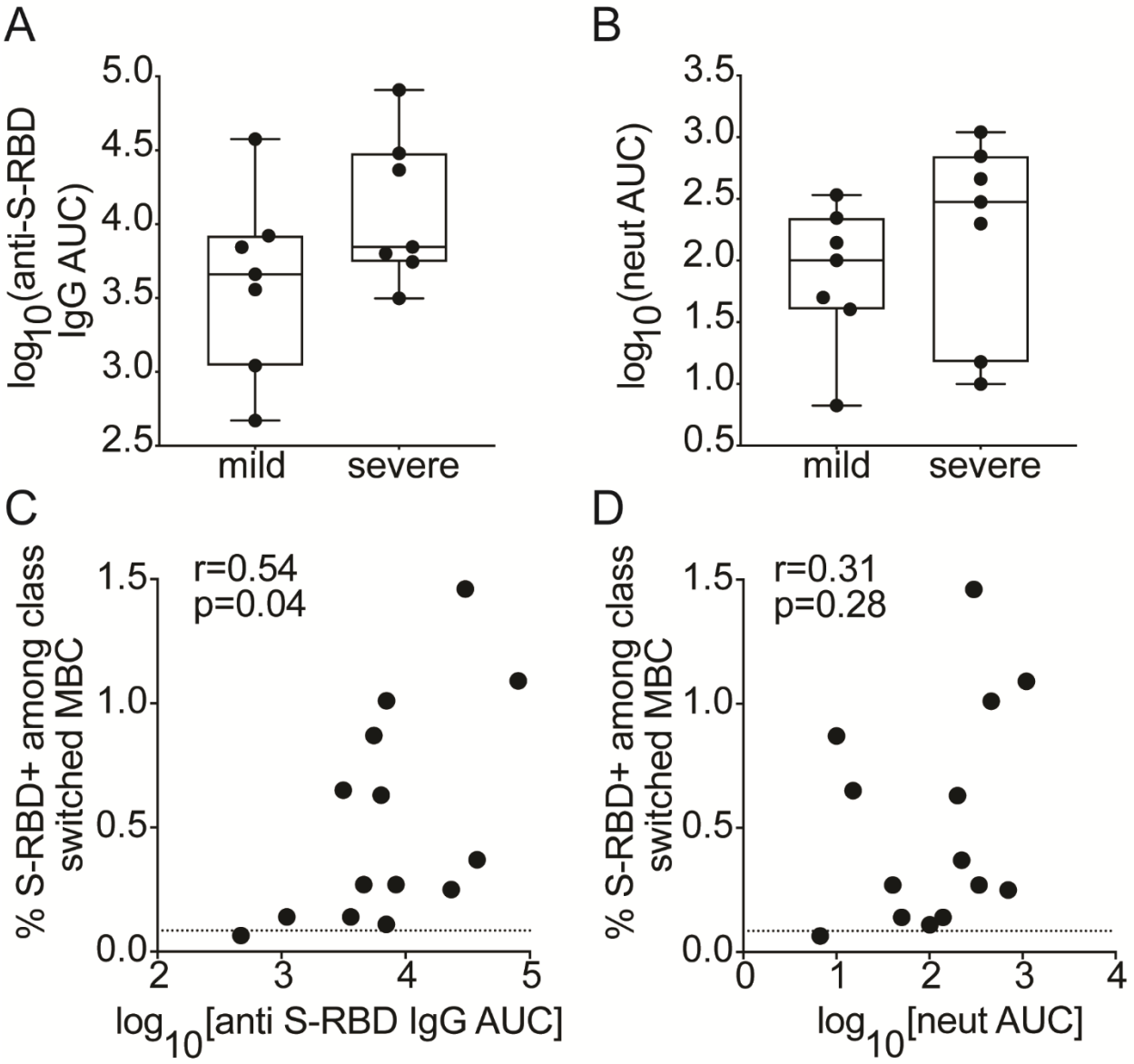

752

753 **Figure 2. Comparisons of serum anti S-RBD IgG and neutralizing antibody titers in mild**
754 **and severe participants. (A)** Anti S-RBD IgG area under the curve (AUC) in mild or severe
755 participants. **(B)** Neutralizing antibody AUC in mild or severe participants. **(C)** Correlation
756 between % of class switched MBC that are S-RBD specific and plasma anti S-RBD IgG AUC
757 from the same subjects. **(D)** Correlation between % of class switched MBC that are S-RBD
758 specific and plasma neutralizing antibody AUC values from the same subjects. Dotted line
759 represents the true S-RBD positive threshold, defined as the mean plus two standard deviations

of the healthy group. For box plots, horizontal lines indicate means, boxes are inter-quartile range, and whiskers are minimum to maximum. Normality of data was confirmed by Shapiro Wilk normality test. Significance in **A**-**B** was calculated using t tests. Correlation r and p values in **C**-**D** were calculated by the Pearson method.

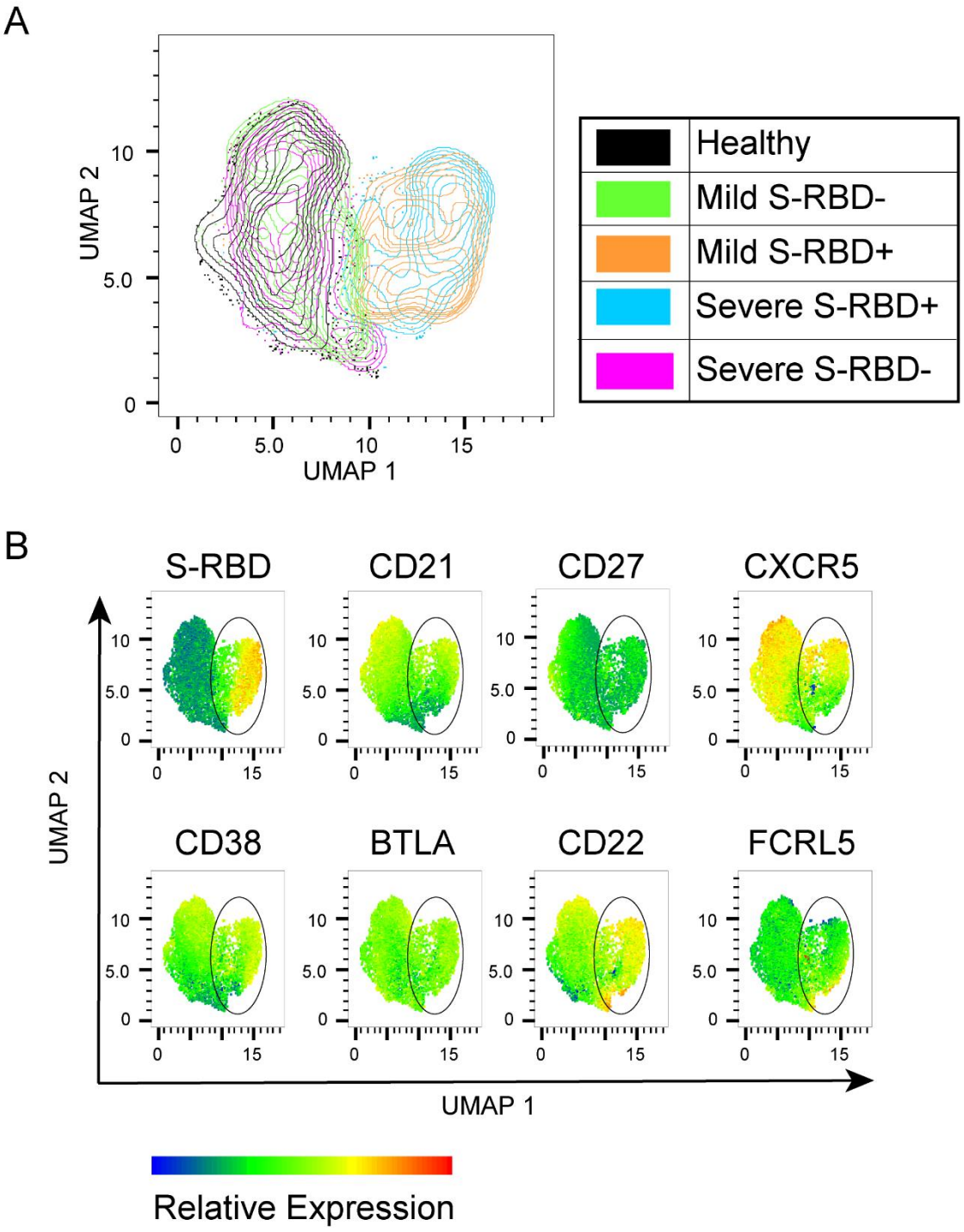

768

769 **Figure 3. UMAP projection of class switched MBC and heatmap statistic of surface**

770 **receptors. (A)** Concatenated class switched MBC from healthy, mild, and severe subjects

projected as a UMAP of S-RBD binding and CD21, CD27, CD38, FcRL5, CD22, CXCR5, and BTLA expression. All S-RBD+ MBC were included, and S-RBD- MBC were downsampled to match S-RBD+ counts for each subject. **(B)** Multigraph color mapping of cell surface receptors on the UMAP projection, with S-RBD+ MBC indicated on each UMAP with a black oval. Lowest expression is indicated by blue and highest expression by red.

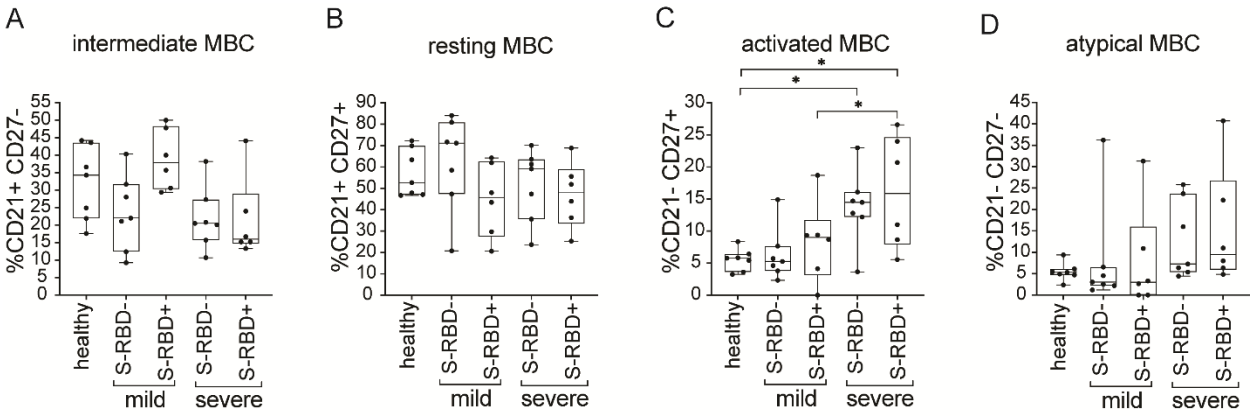

Figure 4. Frequency of MBC subsets in S-RBD nonspecific (S-RBD-) or S-RBD specific (S-RBD+) class switched MBC from healthy, mild, or severe participants. Class switched MBC are defined as CD3-, CD19+, IgM-, IgD-, CD38+/- (excluding ++), CD138- **.** In addition, (**A**) intermediate (intMBC) are CD21+, CD27-; (**B**) classical or resting (rMBC) are CD21+, CD27+; (**C**) activated (actMBC) are CD21-, CD27+; and (**D**) atypical MBC (atyMBC) are CD21-, CD27-. Horizontal lines indicate means, boxes are inter-quartile range, and whiskers are minimum to maximum. Normality of data was determined using Shapiro Wilk normality test, and comparisons were performed using one-way ANOVA for normally distributed data (**B, C**) or Kruskal-Wallis test for non-normally distributed data (**A, D**), with p values adjusted for multiple comparisons using the Benjamini, Krieger and Yekutieli method. Statistically significant comparisons are indicated (* $P \leq 0.05$).

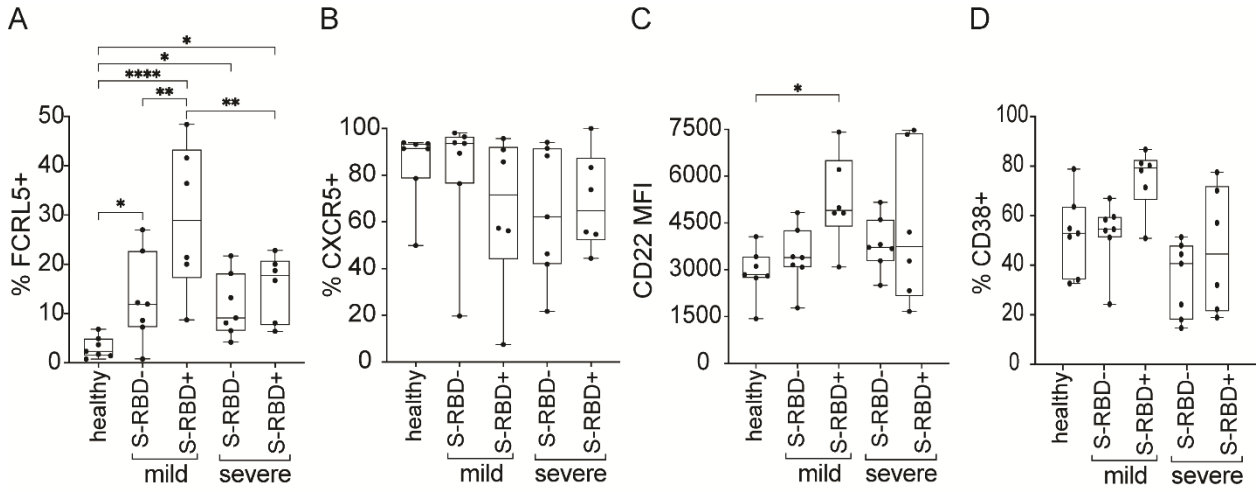

Figure 5. Surface expression of FcRL5, CXCR5, CD22, and CD38 on S-RBD nonspecific (S-RBD-) or S-RBD specific (S-RBD+) class switched MBC from healthy, mild, or severe participants. Expression is shown as either percent of cells positive or the mean fluorescent intensity (MFI). **(A)** FcRL5 **(B)** CXCR5 **(C)** CD22 **(D)** CD38. Horizontal lines indicate means, boxes are inter-quartile range, and whiskers are minimum to maximum. Normality of data was determined using Shapiro Wilk normality test, and comparisons were performed using one-way ANOVA for normally distributed data (**A, C**) or Kruskal-Wallis test for non-normally distributed data (**B, D**), with p values adjusted for multiple comparisons using the Benjamini, Krieger and Yekutieli method. Statistically significant comparisons are indicated (* $P \leq 0.05$, ** $P \leq 0.01$, *** $P \leq 0.001$, **** $P \leq 0.0001$).

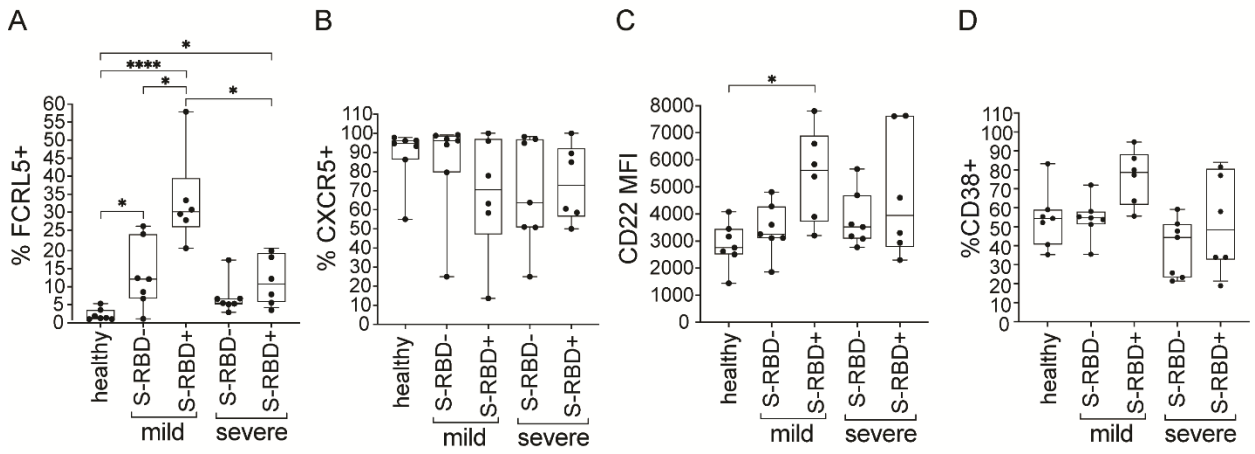

Figure 6. Surface expression of FcRL5, CXCR5, CD22, and CD38 on S-RBD specific (S-RBD+) class switched rMBC (CD21+, CD27+) from healthy, mild, or severe participants. Expression is shown as either percent of cells positive or the mean fluorescent intensity (MFI). **(A)** FcRL5 **(B)** CXCR5 **(C)** CD22 **(D)** CD38. Horizontal lines indicate means, boxes are inter-quartile range, and whiskers are minimum to maximum. Normality of data was determined using Shapiro Wilk normality test, and comparisons were performed using one-way ANOVA for normally distributed data (**C, D**) or Kruskal-Wallis test for non-normally distributed data (**A, B**), with p values adjusted for multiple comparisons using the Benjamini, Krieger and Yekutieli method. Statistically significant comparisons are indicated (* $P \leq 0.05$, **** $P \leq 0.0001$).